



Nano-pyramid-type Co-ZnO/NC for hydrogen transfer cascade reaction between alcohols and nitrobenzene

Chen Wu^a, Changyan Zhu^b, Kangkai Liu^a, Shaowei Yang^a, Yu Sun^a, Kai Zhu^a, Yueling Cao^{a,c}, Sai Zhang^a, Sifei Zhuo^a, Min Zhang^{b,**}, Qiuyu Zhang^{a,**}, Hepeng Zhang^{a,c,*}

^a Xi'an Key Laboratory of Functional Organic Porous Materials, School of Chemistry and Chemical Engineering, Northwestern Polytechnical University, Xi'an, 710129, PR China

^b Institute of Functional Material Chemistry, Faculty of Chemistry, National & Local United Engineering Laboratory for Power Batteries, Northeast Normal University, Changchun, 130024, PR China

^c Research & Development Institute of Northwestern Polytechnical University in Shenzhen, Shenzhen, 518057, PR China

ARTICLE INFO

Keywords:

Catalytic hydrogen transfer
Cascade reaction
Imine synthesis
MOF-derived carbon material
Single atom catalysis

ABSTRACT

The catalytic hydrogen transfer (CHT) cascade reaction between alcohols and nitro- compounds meets green chemistry yet involves high catalyst requirements. Herein, a hierarchical nano-pyramid structure, in which cobalt single atoms (Co SAs) are deposited on highly dispersed ZnO nanoparticles supported by nitrogen-doped carbon (denoted as Co-ZnO/NC), was designed and obtained through pyrolysis of ZnCo-ZIF. The catalyst exhibited excellent catalytic performance toward the CHT cascade reaction, achieving a high nitrobenzene conversion (94 %), imine selectivity (97 %), and turnover frequency (8.8 h^{-1}). This nano-pyramid is a state-of-the-art non-noble-metal catalyst and is comparable to noble-metal catalysts. Experimental and DFT results revealed that the Co SAs supported on ZnO reduced the reaction energy barrier of hydroxyl dehydrogenation, the first and rate-determining step in this heterogeneous catalysis. Furthermore, Co-ZnO/NC exhibits good recyclability and universality. Our findings offer a new catalyst for Schiff base synthesis and aid understanding of the roles of Zn in ZIF-derived carbon catalysts.

1. Introduction

Unsaturated C=N bonds can act as active electrophilic sites in various chemical reactions, including addition, reduction, cyclization, aziridination, and polymerization [1–3]. Therefore, imines as valuable C=N-containing compounds have become essential organic intermediates in biological, pharmaceutical, agricultural, and fine chemical fields [4–9]. Traditionally, imines are synthesized from condensation between carbonyl compounds and amines (Scheme 1a) [10–13]. However, unsaturated ketones and aldehydes are expensive and unstable, and the reactants are not easily accessible, which severely hinders the industrial applications of this approach. In the past few decades, researchers have made unremitting endeavors to pursue atom-economical and environmentally benign synthetic processes to acquire imine products with high selectivities and yields [14–19]. Of such attempts, the oxidative coupling of amines and alcohols holds great

promise for accessibility of imines with water as the only byproduct (Scheme 1b) [20–27]. Furthermore, it would be of significant interest if amines could be substituted with more primitive, cheaper, and more readily available nitro compounds for imine synthesis. In this regard, alcohols can serve as hydrogen donors to efficiently reduce nitroarenes into amines and can also be deprotonated to aldehydes to couple with amines (Scheme 1d). Thus, a one-pot catalytic hydrogen transfer (CHT) cascade reaction between alcohols and nitroarenes has emerged as a powerful method for imine production because it meets atom economy and green synthesis requirements. However, achieving this reaction with high conversions and selectivities is challenging.

Rigorous requirements have been proposed for catalysts toward the CHT cascade reaction, as the catalyst must play roles in both hydrogen deprivation from benzyl alcohol and hydrogen transfer to nitrobenzene. In the last decade, catalysts based on noble metals such as Pd [28,29], Ru [30], and Au [31–33] have been proven to be active in the CHT cascade

* Corresponding author at: Xi'an Key Laboratory of Special Functional & Smart Polymer Materials, School of Chemistry and Chemical Engineering, North-western Polytechnical University, Xi'an, 710129, PR China.

** Corresponding authors.

E-mail addresses: mzhang@nenu.edu.cn (M. Zhang), qyuzhang@nwpu.edu.cn (Q. Zhang), zhanghepeng@nwpu.edu.cn (H. Zhang).

<https://doi.org/10.1016/j.apcatb.2021.120288>

Received 3 March 2021; Received in revised form 24 April 2021; Accepted 30 April 2021

Available online 4 May 2021

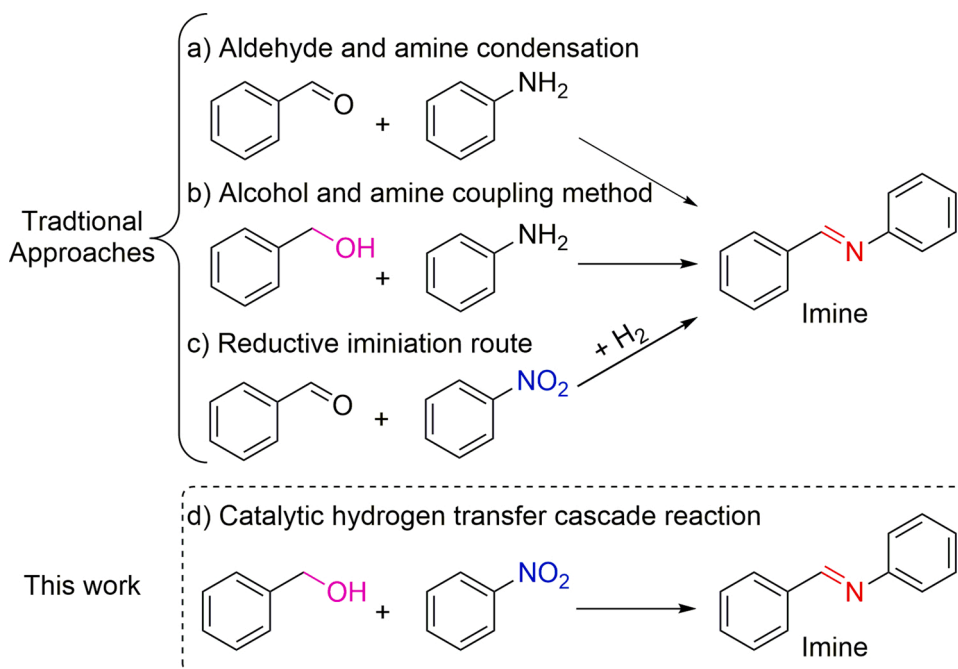
0926-3373/© 2021 Elsevier B.V. All rights reserved.

process. For example, Sankar et al. [31] found that Au-Pd/TiO₂ was capable of catalytically transferring protons from benzyl alcohol to nitrobenzene under an inert atmosphere and achieved an 88 % imine yield after performing the reaction at 160 °C for 3 h with a nitrobenzene/benzyl alcohol molar ratio of 1/10. Despite the effective catalytic performance of this reaction, however, some existing issues, such as the excess required alcohol [31,33] and high costs, have created demand for further exploration. On the other hand, little research on non-noble-metal catalysis has been reported for the coupling between alcohols and nitroarenes due to their low reactivity. Very recently, Liu's group developed a non-noble-metal catalyst based on cobalt nanoparticles (Co-N-C/CNT@AC), obtaining a high imine yield at 160 °C for 18 h [34]. Nevertheless, the prolonged reaction time, complicated catalyst preparation, and low turnover frequency (TOF, 0.6 h⁻¹, based on nitrobenzene conversion and Co amount, wt%, Table S1b) need to be further improved for this catalytic system to be applied industrially. Therefore, it is desirable to develop an efficient and economical non-noble-metal catalyst for the CHT cascade reaction.

According to the CHT cascade reaction, a suitable catalyst should have both acidic and basic sites to serve as active sites for benzyl alcohol adsorption and hydroxyl deprotonation, respectively. Simultaneously, the lattice oxygen in the catalyst should maintain a high stability to avoid the consumption of deprived hydrogen. Zinc oxide (ZnO), an amphoteric oxide that generally act as a base in catalytic reactions, can be implemented as a basic catalyst for alcohol dehydrogenation under an air or oxygen atmosphere, to yield the corresponding carbonyl compounds [35–37]. Furthermore, unlike reducible metal oxides such as CeO₂ and TiO₂, ZnO has an invariable valance state and immobile lattice oxygen, and thus it can stabilize activated hydrogen on its surface and prevent water formation. All these features make ZnO a promising catalyst for the CHT cascade reaction. However, its relatively weak surface acidity restricts hydroxyl adsorption and O–H bond activation, necessitating a high reaction temperature (>250 °C) and aerobic atmosphere [36,37]. These disadvantages could potentially be addressed by reducing the ZnO particle size to expose more active sites and enhance its deprotonation activity [38] or by depositing transition-metal single atoms on ZnO to improve the catalytic activity [39–41]. In this context, we believe that a structure with highly dispersed ZnO nanoparticles supporting transition metal single atoms

would not only increase the surface acidity to improve benzyl alcohol adsorption and weaken the O–H bonds but also maintain the ZnO basic sites for hydroxyl and methylene dehydrogenation. The deprived hydrogens would then be directly transferred to nitroarenes due to the weak mobility of the oxygen species of ZnO. Hence, efficient imine synthesis through the CHT cascade reaction between benzyl alcohol and nitrobenzene would be achieved. However, there have been no examples for such a designed nanohybrid for this reaction.

Herein, a new three-stage nano-pyramid Co-ZnO/nitrogen-doped carbon (NC) material was prepared by calcining a ZnCo-ZIF precursor under an inert atmosphere. In the middle layer of this nano-pyramid, highly dispersed ZnO nanoparticles are supported mainly on the edges of NC (the first floor). Co single atoms (Co SAs), the spire of the nano-pyramid structure, are deposited on the surface of the ZnO nanoparticles. As expected, the prepared Co-ZnO/NC nano-pyramid shows a high catalytic activity toward the CHT cascade reaction between benzyl alcohol and nitrobenzene for imine synthesis. The nitrobenzene conversion and imine selectivity reached 94 % and 97 %, respectively, under an ambient inert atmosphere at 160 °C for 4 h with a theoretical molar ratio of nitrobenzene to benzyl alcohol (1/3). Moreover, the TOF (8.8 h⁻¹) is almost 15 times that reported for other non-noble-metal catalysts under the same reaction conditions (160 °C, N₂) [34]. To the best of our knowledge, Co-ZnO/NC can be ranked as the highest-performing non-noble-metal catalyst for this reaction (Table S1). As demonstrated by experiments and DFT calculations, the bottom NC of the nano-pyramid catalyst contributes to a high ZnO dispersion. Furthermore, due to the strong interaction between the Co SAs and hydroxyl oxygen atoms in the alcohol, the Co SAs supported on ZnO reduce the reaction barrier for hydroxyl dehydrogenation, facilitating the first and rate-determining step of the cascade reaction. The nano-pyramid Co-ZnO/NC catalyst can also be recycled several times without any significant loss in CHT capacity after re-calcination under a N₂ atmosphere. Furthermore, multiple benzyl alcohol and nitrobenzene derivatives could also be transformed into the corresponding imines by Co-ZnO/NC, making it accessible to industrial processes.



Scheme 1. Imine synthetic methods by traditional approaches and CHT cascade reaction.

2. Experimental

2.1. Materials and reagents

Dimethyl imidazole was purchased from Aladdin Reagent Co., Ltd (Shanghai, China). Zinc nitrate hexahydrate ($\text{Zn}(\text{NO}_3)_2 \cdot 6\text{H}_2\text{O}$), cobalt nitrate hexahydrate ($\text{Co}(\text{NO}_3)_2 \cdot 6\text{H}_2\text{O}$), nitrobenzene, benzyl alcohol, toluene, methanol, and ethanol were obtained from Guangdong Guanghua Technology Co., Ltd. Dodecane was purchased from Sigma Company. The above reagents were of analytical grade and used directly without any further purification before the experiment. Deionized water used in the experiments was from local sources.

2.2. Catalyst preparation

2.2.1. Preparation of Zn-ZIF, ZnCo-ZIF, and Co-ZIF

In a typical synthesis procedure, a 7.5 mmol mixture of cobalt nitrate hexahydrate ($\text{Co}(\text{NO}_3)_2 \cdot 6\text{H}_2\text{O}$) and zinc nitrate hexahydrate ($\text{Zn}(\text{NO}_3)_2 \cdot 6\text{H}_2\text{O}$) were dispersed in 75 ml methanol, which was quickly poured into a methanol solution containing 15.0 mmol dimethyl imidazole (MeIM). After 5 min ultrasonic mixing, the slurry was maintained at room temperature for 4 h. The obtained products marked as Zn-ZIF (only zinc addition), ZnCo-ZIF ($\text{Zn}/\text{Co} = 1:1$), and Co-ZIF (only cobalt addition) were washed several times with methanol by centrifugation and dried under vacuum at 60 °C overnight.

2.2.2. Preparation of ZnO/NC, Co-ZnO/NC and Co/NC

The as-synthesized ZIFs were placed in a tubular furnace and heated from room temperature to 900 °C at a heating rate of 5 °C/min and kept for 3 h under N_2 flow.

2.3. Catalyst evaluation

In a typical catalytic hydrogen transfer cascade reaction between nitrobenzene (B) and benzyl alcohol (A), the catalyst (20 mg) was added to the mixture of 1.0 mmol nitrobenzene and 3.0 mmol benzyl alcohol with 1.0 ml toluene as the solvent in a 50 ml Teflon-lined stainless autoclave reactor. The sealed reactor was purged with N_2 three times, and subsequently heated to 160 °C and kept for 4 h.

After the reaction, the mixture was diluted with ethanol and centrifuged. The conversion of the reactant (nitrobenzene) and the yield of the imine product (N-benzylidene aniline, C) were measured by a gas chromatograph (GC, FULI GC 9720) with SE-54 capillary column (30 m \times 0.32 mm \times 0.5 μm) equipped with a flame ionization detector (FID) using dodecane as the internal standard. The operating conditions were as follows: the flow rate of the N_2 carrier gas was 30 mL/min; the injection port temperature was 250 °C. The GC oven temperature program was as follows: first holding at 70 °C for 1 min, then increasing from 70 °C to 240 °C with a heating rate of 12 °C/min, finally holding at 240 °C for 0.5 min.

The nitrobenzene conversion (Con_B) is defined by:

$$\text{Con}_B(\%) = \frac{n_B - n'_B}{n_B} \times 100 \quad (1)$$

and the yield of imine (Yie_C) is calculated based on nitrobenzene conversion by:

$$\text{Yie}_C(\%) = \frac{n'_C}{n_B} \times 100 \quad (2)$$

Hence, the selectivity of imine (Sel_C) based on nitrobenzene conversion could be expressed as:

$$\text{Sel}_C(\%) = \frac{\text{Yie}_C}{\text{Con}_B} \times 100 \quad (3)$$

Where:

n_B : the molar amount of nitrobenzene added in the reaction system, mmol;

n'_B : the molar amount of nitrobenzene in the reaction system after the reaction, mmol;

n'_C : the molar amount of imine in the reaction system after the reaction, mmol.

Catalytic activity per catalyst amount (R_1 , $\text{mmol}_{\text{converted nitrobenzene}} \text{g}^{-1} \text{h}^{-1}$) could be expressed as:

$$R_1 = \frac{n_B \cdot \text{Con}_B\%}{m \cdot t} \quad (4)$$

Catalytic activity per metal amount (R_2 , $\text{mmol}_{\text{converted nitrobenzene}} \text{g}_{\text{metal}}^{-1} \text{h}^{-1}$) could be expressed as:

$$R_2 = \frac{n_B \cdot \text{Con}_B\%}{(\text{Zn wt}\% + \text{Co wt}\%) \cdot m \cdot t} \quad (5)$$

Turnover frequency (TOF, $\text{mmol}_{\text{converted nitrobenzene}} \text{mmol}^{-1} \text{h}^{-1}$) could be expressed as:

$$\text{TOF} = \frac{n_B \cdot \text{Con}_B\%}{\left(\frac{\text{Zn wt}\%}{M_{\text{Zn}}} + \frac{\text{Co wt}\%}{M_{\text{Co}}} \right) \cdot m \cdot t} \quad (6)$$

Where:

n_B : the molar amount of nitrobenzene added in the reaction system, mmol;

Con_B : the nitrobenzene conversion was determined by GC using dodecane as an internal, %;

$\text{Co wt}\%$ and $\text{Zn wt}\%$: the cobalt and zinc contents in the catalysts which are determined by ICP-MS;

M_{Co} : the molar mass of Co, 58.93 g/mol;

M_{Zn} : the molar mass of Zn, 65.41 g/mol;

m : the mass amount of the catalysts added in the reaction system, g;

t : reaction time, h.

2.4. Characterization

Powder X-ray diffraction patterns of both ZIF and carbon materials were recorded on a Bruker D8 DISCOVER A25 X-ray diffractometer (Germany) with $\text{Co K}\alpha$ radiation (3 kV). The samples' morphology and structure were studied using field-emission scanning electron microscope (FE-SEM, FEI Verious G4) and transmission electron microscopy (TEM, FEI Talos F200X TEM operated at 200 kV). Co and Zn contents were obtained on Inductively Coupled Plasma Mass Spectrometer (ICP-MS, NexION™ 350D PerkinElmer USA). X-ray diffraction patterns (XRD) were recorded using X-ray powder diffraction (XRD-7000S from Shimadzu) to characterize the structure and crystallinity of the samples. N_2 -adsorption desorption isotherms and pore size distributions were obtained using the 3H-2000PS2 type PS2-0790 Surface Area Porosity Analyzer from Beishide Instrument Technology (Beijing) Co., Ltd. The samples were degassed at 80 °C for 4 h under vacuum before testing. The specific surface area and pore volume were calculated from the Brunauer-Emmett-Teller (BET) and Barrett-Joyner-Halenda (BJH) methods, respectively. X-ray photoelectron spectroscopy (XPS) measurements were performed with an Axis Ultra DLD X-ray photoelectron spectroscopy manufactured by Kratos Company in the United Kingdom. The instrument used an Al $\text{K}\alpha$ ray light source to measure the total ambient gas pressure ($<10^{-8}$ Pa). NH_3 temperature-programmed desorption (NH_3 -TPD) and CO_2 temperature-programmed desorption (CO_2 -TPD) were carried out on a Micromeritics Autochem II chemisorption analyzer. 50 mg sample loaded in a quartz reactor was pre-treated with Ar at 500 °C. After cooling to 50 °C, NH_3 or CO_2 adsorption was performed by switching Ar to NH_3 or CO_2 gas and then maintaining 2 h. After adsorption, the physical adsorption of NH_3 or CO_2 was removed at the same temperature by Ar purging for 1 h. Then, TPD was detected by Thermal Conductive Detector (TCD) in the Ar flow by

raising the temperature to 700 °C at a rate of 10 °C/min. *in situ* diffuse reflectance infrared spectroscopy of carbon monoxide adsorption (CO-DRIFTS) was recorded on a Bruker Optics VERTEX 70 equipped with a liquid nitrogen-cooled MCT detector and a PIKE Diffuse IR chamber, using an *in situ* IR cell equipped with ZnSe windows, which was connected to a conventional gas flow system. The recorded spectra consisted of 32 scans at 4 cm⁻¹ resolution. Before CO adsorption, the catalysts powders (~20 mg) were put into the DRIFTS cell under a 10 v% H₂/Ar flow (30 mL/min) and pretreated at 350 °C for 2 h, followed by Ar purge (30 mL/min) for another 1 h, and then cooled down to 30 °C to collect background. Thereafter, the sample was exposed under 5 v% CO/Ar (30 mL/min) for 15 min.

2.5. DFT calculations

The structure optimizations were performed by spin-polarized density functional theory (DFT) using Vienna ab initio simulation package (VASP). The generalized gradient approximation of Perdew-Burke-Ernzerhof (GGA-PBE) was employed to describe the electronic exchange-correlation effects. The projector augmented wave (PAW) pseudo potential was applied to take the ion-electron interactions into account. The valence density was expanded in a plane-wave basis set with a kinetic energy cutoff of 400 eV. The Grimme's semiempirical DFT-D3 approach was chosen for the van der Waals interaction between reaction intermediates and substrate. The climbing-image nudged elastic band (CI-NEB) method was adopted to search for the saddle point and the optimal reaction pathway. The vacuum distance of 15 Å along the z direction was used to minimize interaction between periodically repeated slabs. The structures were relaxed with the energy converged of 10⁻⁵ eV, and the force converged of 0.02 eV Å⁻¹ for each atom, respectively.

2.6. Structural model

The optimized lattice constants of bulk ZnO are *a* = 3.247 Å and *c* = 5.253 Å using 14 × 14 × 8 Monkhorst pack k-points mesh, which is in good agreement with the experimentally measured values (*a* = 3.249 Å and *c* = 5.210 Å). A four-unit-layer slab with a 3 × 2 supercell was modeled the ZnO (100) surface, which contains 48 Zn atoms and 48 O atoms. The bottom two layers of the ZnO (100) slab were fixed at their crystal lattice positions while the adsorbate and the top layers of the ZnO (100) slab were allowed to relax fully. A 5 × 4 × 1 Monkhorst pack k-points mesh was applied to sample the Brillouin zone of the supercells.

3. Results and discussion

3.1. Catalyst synthesis and characterizations

As shown in Fig. 1, the nano-pyramid Co-ZnO/NC catalyst was fabricated via a two-step process: (1) synthesis of ZnCo-ZIF with an appropriate Zn/Co ratio and (2) controlled pyrolysis of the ZnCo-ZIF precursor at 900 °C in a N₂ atmosphere to prepare the nano-pyramid Co-ZnO/NC hybrid. X-ray diffraction (XRD, Fig. S1) patterns and N₂ sorption isotherms (Fig. S2 and Table S2) confirmed that the ZnCo-ZIF precursor possessed a ZIF-8 structure with micropores. Scanning electron microscopy (a1, Fig. 2) and transmission electron microscopy (TEM, a2, Fig. 2) revealed that ZnCo-ZIF had a well-defined rhombic dodecahedral shape with smooth surfaces and a uniform size distribution, and after pyrolysis, the obtained Co-ZnO/NC preserved the rhombic dodecahedral morphology (Fig. 2b). High-angle annular dark-field scanning TEM (HAADF-STEM) and STEM energy dispersive X-ray (STEM-EDX) elemental analysis (Fig. 2c) of Co-ZnO/NC showed no notable large inorganic particles, and the observed Zn and Co were highly dispersed. This was further confirmed by the XRD pattern of Co-ZnO/NC (Fig. 2f), which lacked any characteristic signals of Zn, Co, or ZnO. In contrast, the further aberration-corrected TEM images (Fig. 2d) exhibited multiple small particles (2–5 nm) located mainly on the edges of the NC with clear lattice fringes. The interplanar distances measured as 0.281, 0.260, and 0.247 nm correspond to the (100), (002), and (101) planes of ZnO, respectively, demonstrating that the small particles are single-crystal ZnO. The existence of ZnO was also proven by X-ray photoelectron spectroscopy (XPS, Fig. 2g), where the prominent peaks in the Zn 2p spectrum of Co-ZnO/NC appeared at approximately 1021.4 eV (Zn 2p_{3/2}) and 1044.4 eV (Zn 2p_{1/2}), suggesting an electronic state of Zn²⁺ [42]. Moreover, as shown in the HAADF-STEM and STEM-EDX images (Fig. 2e), several relatively bright spots were recognized as Co SAs distributed on the surface of the ZnO nanocrystals. The Co 2p spectrum (Fig. 2h) also revealed no distinct peaks belonging to Co⁰ species on Co-ZnO/NC, further confirming the existence of Co SAs on the surface of ZnO. Moreover, the existing of Co SAs was also validated through CO DRIFTS spectra of the Co-ZnO/NC (Fig. S3) by the broad peaks at 2235 and 2138 cm⁻¹ attributing to linear adsorption of CO on oxidized cobalt species (Co²⁺ and Co³⁺) [43–45]. Accordingly, we constructed a hierarchical nano-pyramid-like hybrid composed of Co SAs supported by highly dispersed ZnO nanoparticles loaded on the edge of NC. The BET surface areas (Fig. S2 and Table S3) of the ZnCo/NC materials displayed a decreasing trend along with the increase of Co content in the following order: ZnO/NC (904 m²/g) > Co-ZnO/NC (820 m²/g) > Co/NC (246 m²/g), which may be derived from the highly dispersion of ZnO species in both ZnO/NC and Co-ZnO/NC catalysts and

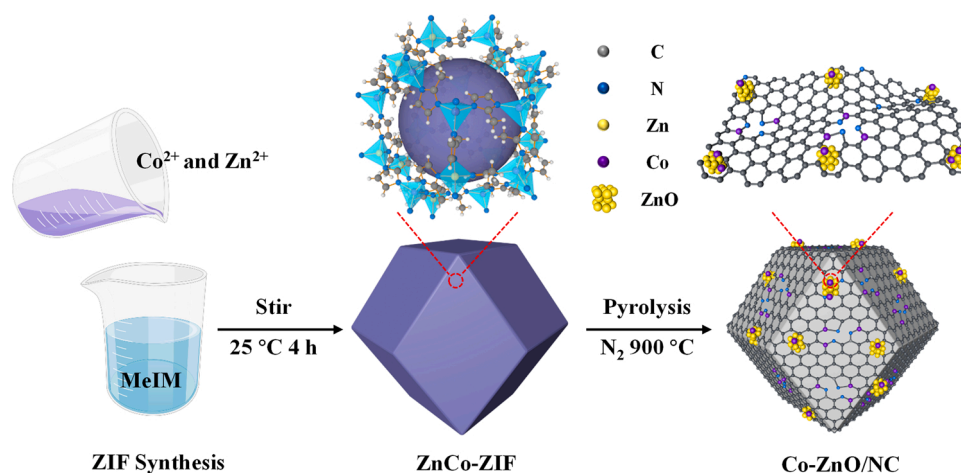


Fig. 1. Schematic illustration of the Co-ZnO/NC synthesis.

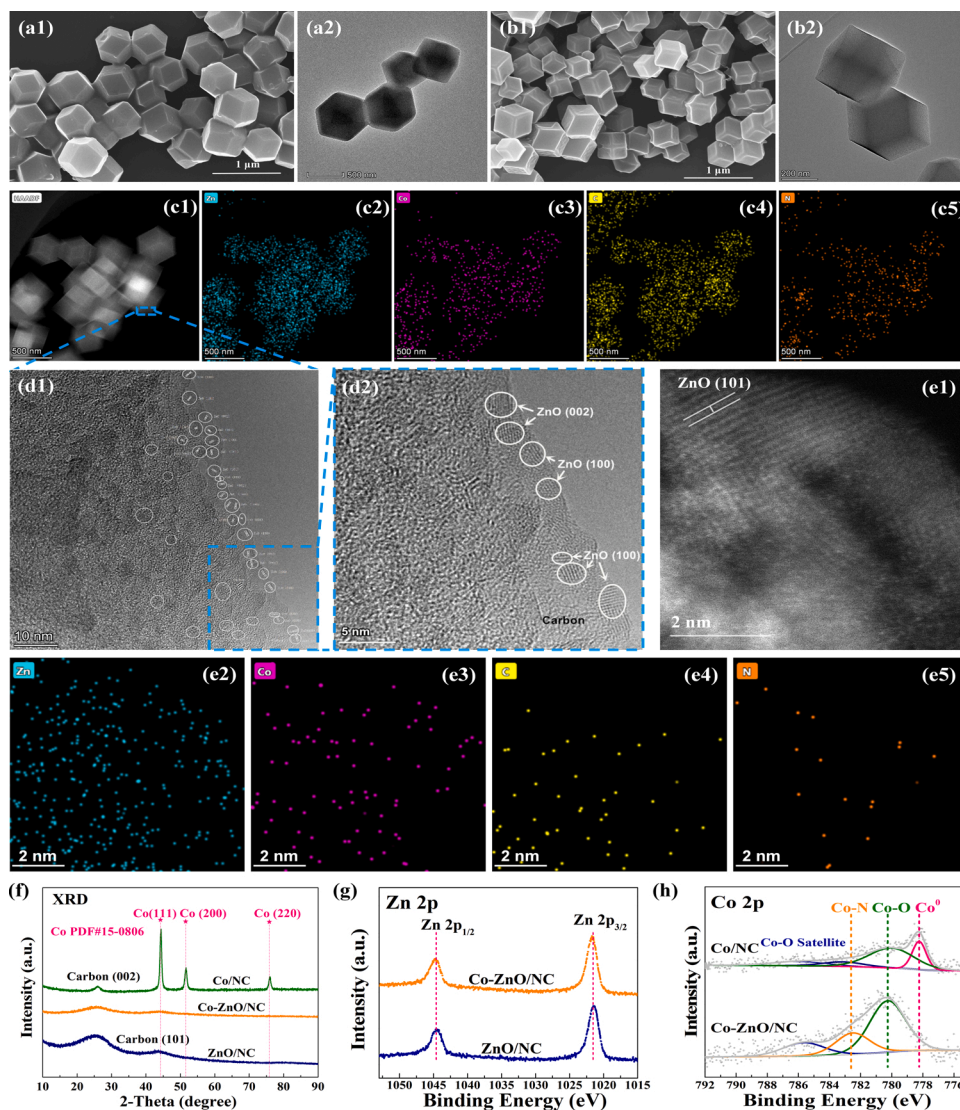


Fig. 2. (a1) SEM and (a2) TEM images of ZnCo-ZIF; (b1) SEM and (b2) TEM images of Co-ZnO/NC; (c) HADDF-STEM image (c1) and corresponding STEM-EDX elemental analysis showing elements distribution of Co-ZnO/NC: Zn (cyan, c2), Co (purple, c3), C (yellow, c4) and N (orange, c5), respectively; (d) aberration-corrected TEM image of Co-ZnO/NC (d1) and magnified image (d2) of the selected area; (e) HADDF-STEM image (e1) and corresponding STEM-EDX elemental analysis showing elements distribution of edges from Co-ZnO/NC: Zn (cyan, e2), Co (purple, e3), C (yellow, e4) and N (orange, e5), respectively; (f) XRD, (g) Zn 2p, and (h) Co 2p of the obtained NCs. (For interpretation of the references to colour in this figure legend, the reader is referred to the web version of this article).

the agglomeration of cobalt species in the Co/NC catalyst.

3.2. Catalytic performance toward CHT cascade reaction

The CHT cascade reaction for imine synthesis was performed at 160 °C for 4 h under a N₂ atmosphere with a nitrobenzene to benzyl alcohol molar ratio of 1/3. As expected, the nitrobenzene conversion and imine yield reached 94 % and 91 %, respectively, over Co-ZnO/NC. No aniline was detected in any of the obtained reaction mixtures, and the secondary amine yield was 3%, indicating excellent selectivity toward the target imine. A straightforward comparison of Co-ZnO/NC with reported catalysts (Table S1) confirmed that the new nano-pyramid is a state-of-the-art non-noble-metal catalyst for the CHT cascade reaction, with a catalytic capacity rivaling even that of several reported noble-metal catalysts. The excellent catalytic performance of Co-ZnO/NC verified our initial idea that highly dispersed ZnO nanoparticles supporting transition-metal SAs would benefit the CHT cascade reaction for imine synthesis from benzyl alcohol and nitrobenzene. In addition, TOF (Eq. (6)) was calculated based on the total metal contents. The TOF achieved by Co-ZnO/NC (calculated as 8.8 h⁻¹) is one order of magnitude higher than that of the reported Co-N-C/CNT@AC catalyst (0.6 h⁻¹, Table S1b) [34] under the same reaction conditions.

ZnO/NC and Co/NC, obtained through the pyrolysis of Zn-ZIF and Co-ZIF precursors, respectively, were also used to catalyze the CHT

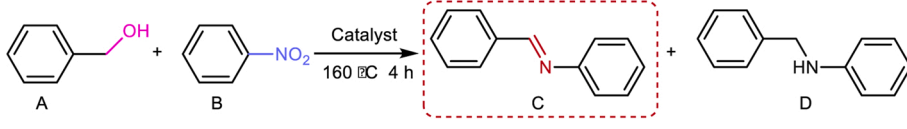
reaction. As suggested by TEM and HR-TEM (Figs. S4 and S5), ZnO/NC, like Co-ZnO/NC, contained ZnO nanoparticles on the edges of the NC, whereas metallic Co nanoparticles were identified on Co/NC. XRD (Fig. 2f) and XPS (Fig. 2g and h) further verified the presence of ZnO and metallic cobalt on ZnO/NC and Co/NC, respectively. Both catalysts were active toward the CHT cascade reaction between alcohol and nitrobenzene (Tables 1 and S4), indicating that ZnO and metallic cobalt species could also serve as active sites for the reaction. However, their catalytic performances were inferior to that of Co-ZnO/NC.

3.3. Catalytic sites and rate-determining step verification

To determine the main catalytic sites in the nano-pyramid Co-ZnO/NC, a series of Zn, Co, and carbon-based samples were chosen to catalyze the CHT cascade reaction for imine synthesis (Table S5). The pristine ZIF material showed no catalytic performance toward this reaction. Activated carbon (AC) and NC exhibited deficient catalytic activities, indicating that the NC in Co-ZnO/NC mainly functions as a catalyst support for the dispersion of ZnO nanoparticles. The other characterizations further verifying the effect of NC species are illustrated in Supplementary Material (Fig. S6). Moreover, compared with Co-ZnO/NC and ZnO/NC, bulk ZnO particles, CoO, and Co particles also showed low nitrobenzene conversions, whereas ZnO supported by AC exhibited slightly improved catalytic performance, proving that a high dispersion of active

Table 1

CHT cascade reaction results between nitrobenzene and benzyl alcohol catalyzed by the obtained materials.

									
Entry	Catalyst	Zn wt%	Co wt%	Con _B %	Se _C %	Se _D %	R ₁ ^[a] mmol h ⁻¹ g ⁻¹	R ₂ ^[b] mmol h ⁻¹ g ⁻¹	TOF ^[c] h ⁻¹
1	ZnO/NC	9.3	–	41	85	15	5.1	5510	3.6
2	Co-ZnO/NC	6.5	2.0	94	97	3	11.8	13823	8.8
3	Co/NC	–	38.2	56	95	5	6.6	1832	1.1
4	ZnO/NC-H-24	4.6	–	21	71	29	2.6	5707	3.7
5	Co-ZnO/NC-H-24	3.6	1.2	22	95	5	2.8	5729	3.6
6	Co/NC-H-24	–	3.8	4	100	0	0.5	1315	0.7

Reaction conditions: 3 mmol benzyl alcohol, 1 mmol nitrobenzene, 20 mg catalyst, 1 ml toluene, 160 °C, 4 h, N₂. The conversion and yield were determined by GC. [a] Reaction activity based on catalyst amount, mmol h⁻¹ g⁻¹; [b] Reaction activity based on total metal amounts, mmol h⁻¹ g⁻¹; [c] TOF was calculated based on the total metal molar amounts (Zn and Co) in the catalysts and nitrobenzene conversion, h⁻¹.

components is essential for a high catalytic performance.

Subsequently, acid-etching experiments that could destroy the surface ZnO or Co-ZnO particles were performed to further ascertain the catalytic active sites of Co-ZnO/NC. Co-ZnO/NC was immersed in a 0.5 M H₂SO₄ aqueous solution for several hours (denoted as Co-ZnO/NC-H-*t*). As shown in Fig. 3a, H₂SO₄ etching of the catalyst greatly hindered its CHT performance, as Co-ZnO/NC lost 40 % of its hydrogen transfer ability with only 30 min of etching. As the etching time increased, the nitrobenzene conversion and imine yield declined gradually, and after etching for 24 h, Co-ZnO/NC-H-24 showed only a 22 % nitrobenzene conversion. Further elevating etching temperature could

not completely deactivate the catalyst, as it maintained a nitrobenzene conversion into imine of approximately 20 % (Table S6). Moreover, the nitrobenzene conversions of ZnO/NC-H-24 and Co/NC-H-24 were reduced to 21 % and 4 %, respectively (Table 1).

The inductively coupled plasma mass spectrometry results (Table 1) of the etched catalysts revealed that residual metals remained even after etching for 24 h. The HAADF-STEM images (Fig. S7) confirmed that these metallic species were in the form of Zn/Co SAs on NC or carbon-encapsulated metal/metal oxide nanoparticles. The Zn/Co SAs on the NC might account for the remaining catalytic activity of Co-ZnO/NC-H-24 due to the carbon-encapsulated metal/metal oxide could not connect

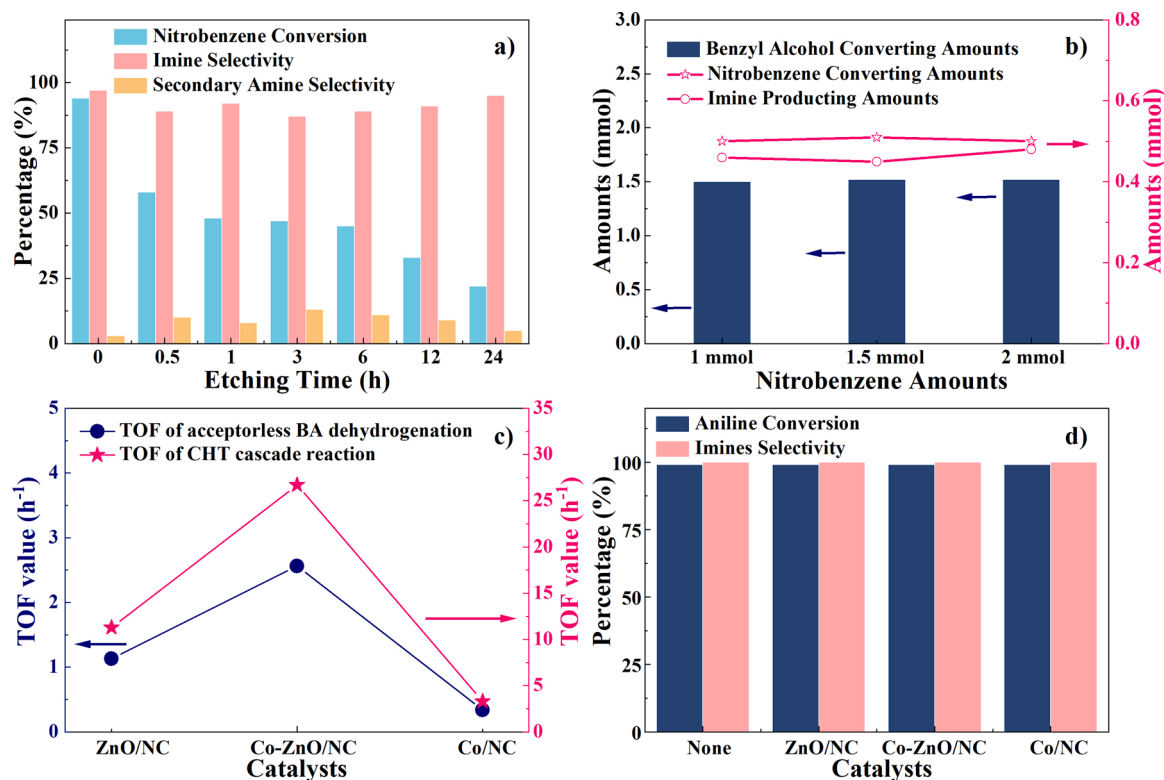


Fig. 3. (a) Catalytic performance of catalyst etched by H₂SO₄ aqueous for different times, conditions: 3 mmol benzyl alcohol, 1 mmol nitrobenzene, 20 mg catalyst, 1 ml toluene, 160 °C, 4 h, N₂; (b) Reaction results for CHT cascade reaction over Co-ZnO/NC by changing nitrobenzene amounts, conditions: 3 mmol benzyl alcohol, 20 mg catalyst, 1 ml toluene, 0.5 h, 160 °C, N₂; (c) TOF comparison of the three catalysts on the benzyl alcohol (BA) acceptorless dehydrogenation and the CHT cascade reaction, conditions: 3 mmol benzyl alcohol, 20 mg catalyst, 1 ml toluene, 4 h, 160 °C, N₂, the TOF values were calculated based on the benzyl alcohol conversions; (d) Reaction results of coupling between aniline and benzaldehyde under an inert atmosphere, conditions: 3 mmol benzaldehyde, 1 mmol nitrobenzene, 20 mg catalyst, 1 ml toluene, 160 °C, 4 h, N₂.

with reactants during the reaction process. The metal losses were 4.7 wt % (Zn content) for ZnO/NC-H-24 and 3.7 wt% (Zn and Co contents) for Co-ZnO/NC-H-24, whereas their corresponding catalytic activities declined by 20 % and 72 %, respectively. These results further support that the Co SAs deposited on highly dispersed ZnO nanoparticles were the main catalytic active sites and accounted for approximately 72 % of the 94 % nitrobenzene conversion of the nano-pyramid Co-ZnO/NC catalyst, which is almost 3.5 times that of the highly dispersed ZnO (20 %) in ZnO/NC.

Several comparative experiments were carried out to explore the functions of the Co-ZnO active sites and elucidate the reaction mechanism of the CHT cascade process over Co-ZnO/NC. Initially, the amount of the nitrobenzene reactant was altered. As shown in Fig. 3b, when the nitrobenzene amount was increased from 1 to 2 mmol, the benzyl alcohol and nitrobenzene conversion rates and imine production amounts exhibited negligible vibrations. This indicated that the nitrobenzene molecule does not participate in the rate-determining elementary reaction step and that nitrobenzene hydrogenation could occur swiftly once the protons were removed from benzyl alcohol by the catalyst. Hence, it could be preliminarily deduced that benzyl alcohol dehydrogenation into benzaldehyde is the rate-determining step.

To verify this inference, benzyl alcohol dehydrogenation under an inert atmosphere with no hydrogen acceptor was carried out. All three catalysts demonstrated low dehydrogenation performances (benzyl alcohol conversions <10 %), compared with the benzyl alcohol conversions (>40 %) obtained during the CHT cascade process. This is because the hydrogen deprived from benzyl alcohol occupied the active sites of the catalysts when no hydrogen acceptor (such as nitrobenzene)

was present in the reaction system, and thus the continuous dehydrogenation of benzyl alcohols was inhibited. On the other hand, the TOF trend for benzyl alcohol dehydrogenation (Fig. 3c, Co-ZnO/NC > ZnO/NC > Co/NC) was almost the same as that of the CHT cascade reaction, further confirming that benzyl alcohol dehydrogenation into benzaldehyde is the rate-determining step. Moreover, the coupling between aniline and benzaldehyde proceeded rapidly even without the catalyst, and the three catalysts exhibited indistinct behaviors toward the reaction (Fig. 3d). Experimental time tracking of the reaction demonstrated trace amounts of aniline (4 %) in the early period, whereas no aniline was present after reacting for 2 h (Fig. S8), further confirming that the coupling between aniline and benzaldehyde was rapid. These results confirm that benzyl alcohol dehydrogenation is the rate-determining step in this CHT cascade reaction.

3.4. DFT calculations

DFT calculations were performed to interpret the role of the decorated Co SA on the ZnO surface in improving the catalytic activity for benzyl alcohol dehydrogenation. Based on TEM observations and the stability of the hexagonal zincite faces, the ZnO (100) facet was selected for the simulation (a1, Fig. 4). A single Co atom preferred to be between two O atoms of the ZnO (100) facet with a Co-O bond length of 1.77 Å after optimizing various structures (a2, Fig. 4). To evaluate the structural stability, the binding energy ($\Delta E_{\text{binding,Co}}$) was first calculated by $\Delta E_{\text{binding,Co}} = E_{\text{Co/ZnO}} - E_{\text{ZnO}} - E_{\text{Co}}$, where $E_{\text{Co/ZnO}}$, E_{ZnO} , and E_{Co} are the total energies of the ZnO (100) facet with and without the decorated Co atom and an isolated Co atom, respectively. The results demonstrated

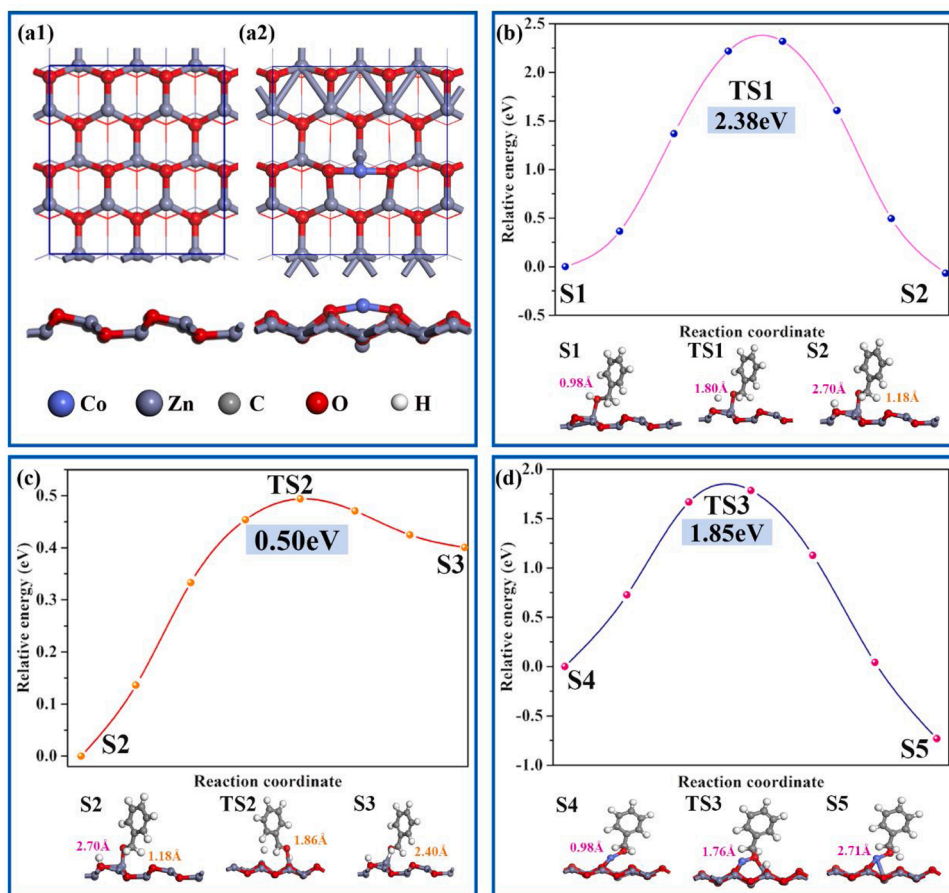


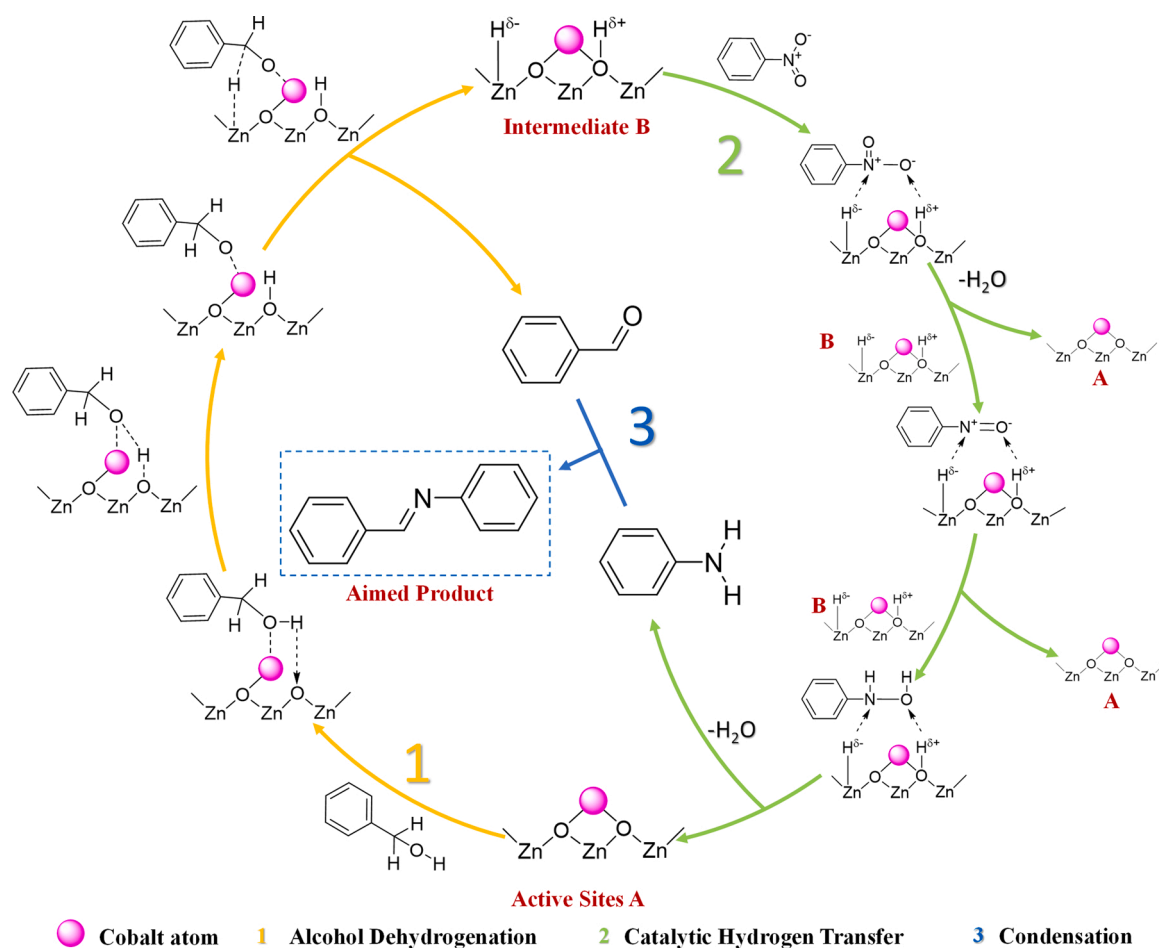
Fig. 4. (a) Top and side view of ZnO (100) (a1) and Co/ZnO (100) (a2). (b) Potential energy profile for the dehydrogenation of hydroxyl on the ZnO (100). (c) Potential energy profile for the dehydrogenation of benzyloxy on the ZnO (100). (d) Potential energy profile for the dehydrogenation of hydroxyl on the Co/ZnO (100). S and TS: Optimized structures of the equilibrium geometries and the connected transition states.

that a single Co atom can stably anchor on the ZnO (100) facet with a calculated binding energy of -2.42 eV. Moreover, there is a significant charge transfer ($0.59|e|$) from the decorated Co atom to the ZnO (100) facet based on Bader charge analysis. It was also found that a strong interaction occurs between the decorated Co atom and ZnO (100) facet, which is crucial for the subsequent dehydrogenation of benzyl alcohol. According to the previous discussion, benzyl alcohol dehydrogenation is the rate-determining step in the CHT cascade reaction. Thus, to save computing resources, only the dehydrogenation reactions of benzyl alcohol to benzaldehyde on the pure ZnO (100) and Co/ZnO (100) facets were investigated.

On the pure ZnO (100) facet, benzyl alcohol can adsorb on the Zn atom via the hydroxyl oxygen atom with a Zn–O distance of 2.13 Å (S1, Fig. 4b). Moreover, the O–H bond length (0.98 Å) of the hydroxyl group in the adsorbed benzyl alcohol is slightly longer than that (0.97 Å) of the isolated benzyl alcohol molecule, suggesting that the O–H bonding has been activated. The activated hydroxyl H atom shifts to the adjacent O atom of the ZnO (100) facet during the first dehydrogenation reaction, which must overcome a high activation barrier of 2.38 eV (Fig. 4b). In the first dehydrogenation reaction, the hydroxyl O–H distance elongates to 1.80 Å in the transition state (TS1, Fig. 4b) from the initial distance of 0.98 Å in the reactant (S1, Fig. 4b) and reaches 2.70 Å in the product (S2, Fig. 4b), which demonstrates that the hydroxyl H atom completely shifts to the ZnO (100) facet. In the second dehydrogenation reaction, another methylene H atom shifts to the adjacent Zn atom, which only needs to overcome a much lower activation barrier of 0.50 eV (Fig. 4c). In this dehydrogenation process, the methylene C–H distance changes to 1.86 Å in the transition state (TS2, Fig. 4c) from the initial 1.18 Å in the reactant (S2, Fig. 4c), and then reaches 2.40 Å in

the product (S3, Fig. 4c), which demonstrates that the methylene H atom has also completely shifts to the ZnO (100) facet. In this two-step dehydrogenation reaction, the first is the rate-limiting step due to its higher activation barrier. Therefore, it is crucial to diminish the activation barrier of the first step to improve the catalytic activity toward benzyl alcohol dehydrogenation.

The activation barrier of the first dehydrogenation reaction on the Co/ZnO (100) facet was further calculated to interpret the experimental observations. As expected, the activation barrier decreased to 1.85 eV (Fig. 4d) after a single Co atom was anchored on the ZnO (100) facet. These data are in good agreement with the experimental observations and suggest that the Co atom can facilitate hydroxyl dehydrogenation and improve the catalytic activity. In contrast to the process on the pure ZnO (100) facet, benzyl alcohol can adsorb on the Co atom via the oxygen atom of the hydroxyl group with a Co–O distance of 1.91 Å (S4, Fig. 4d). However, the optimized hydroxyl O–H bonding length (0.98 Å) in the adsorbed benzyl alcohol and the change of O–H bonding length in the first dehydrogenation reaction (0.98 Å in reactant S4, Fig. 4d; 1.76 Å in transition state TS3, Fig. 4d; and 2.71 Å in product of S5, Fig. 4d) are identical to those on the pure ZnO (100) facet. Most importantly, the relative energy of product S5 is 0.73 eV below that of reactant S4 after the first dehydrogenation, indicating a more vital interaction between the product and anchored Co atom after removing the H atom from the hydroxyl group. This strong interaction arising from the adsorbed Co atom is an intrinsic factor in decreasing the activation energy of the first dehydrogenation reaction and enhancing the catalytic activity toward benzyl alcohol dehydrogenation.



Scheme 2. Proposed CHT cascade reaction mechanism over Co-ZnO/NC.

3.5. Catalytic mechanism

Combining the experimental results and DFT calculations, the proposed reaction mechanism over Co-ZnO/NC is illustrated in Scheme 2. Owing to the electronic structure and bonding with two lattice oxygen atoms of ZnO, Co has a stronger acidity than Zn^{2+} in Co-ZnO (active site A, Scheme 2). NH_3 temperature-programmed-desorption (Fig. S9) also confirmed this conclusion. Accordingly, the O atom of benzyl alcohol hydroxyl group can be preferentially drawn to the Co atom at active site A (step 1, Scheme 2). Subsequently, H^+ from the hydroxyl group transfers to the adjacent O atom due to the strong interaction between the Co atom and hydroxyl O atom. Finally, $\alpha\text{-H}$ from the benzyloxy methylene group is deprived to Zn^{2+} in the form of H^- , forming intermediate B and simultaneously producing benzaldehyde.

For the CHT reaction (step 2, Scheme 2), it has been reported that the hydrogenation of nitrobenzene to aniline follows three main steps [46–50]. First, PhNO_2 obtains two electrons and two H atoms to form PhNO (nitrosobenzene), PhNO is hydrogenated into PhNHOH (phenylhydroxylamine) by two electrons and two H atoms, and finally PhNH_2 (aniline) forms via PhNHOH reduction through a similar process. During the CHT route in our catalytic system, the electron-deficient N atom in nitrobenzene attracts a pair of electrons from the $\text{H}^{\delta-}$ of intermediate B and further removes the $\text{H}^{\delta+}$ from B. Then, PhNO_2 is hydrogenated into the PhNO intermediate. Meanwhile, active site A is exposed for the next circulation of benzyl alcohol dehydrogenation. The PhNO intermediate further reacts with another pair of $\text{H}^{\delta-}$ and $\text{H}^{\delta+}$ from the newly formed intermediate B, which is reduced to PhNHOH . Finally, PhNHOH is converted to PhNH_2 through a similar hydrogenation process. Once aniline forms, it immediately reacts with benzaldehyde to yield the target imine (step 3, Scheme 2) [22].

The CHT reaction mechanism between benzyl alcohol and nitrobenzene over Co/NC catalyst is also proposed, the details are shown in Scheme S1.

3.6. Catalyst recyclability and universality

Recycling tests were implemented to examine the reusability and stability of the Co-ZnO/NC nanohybrid (Fig. S10). After three cycles, the nitrobenzene conversion and imine selectivity decreased from 94 % and 97 % to 74 % and 91 %, respectively. However, the TEM images (Fig. S11) of the recycled nano-pyramid catalyst after three cycles displayed no structural agglomeration or destruction, which suggests that the loss of the reactivity of Co-ZnO/NC mainly stems from the coverage of active sites by the adsorption of organic reactants and products. In addition, the reactivity can easily be recovered by high-temperature pyrolysis [51]. Indeed, the recycled catalyst regained its catalytic hydrogen transfer activity after re-calcining under N_2 at 900 °C for 3 h.

Other aromatic alcohols and substituted nitrobenzene derivatives were selected as reactants to determine the scope of the CHT cascade reaction over the nano-pyramid Co-ZnO/NC catalyst. Interestingly, Co-ZnO/NC exhibited a much higher catalytic capacity than other reported non-noble-metal catalysts for imine derivatives [34]. As listed in Table 2, the hydrogen atoms from aromatic alcohols with different substituents and heteroaromatic alcohols could all be transferred to nitrobenzene, yielding the corresponding imines smoothly (entries 2f–8f). Moreover, the reaction activities of alcohols with electron-donating groups were higher than those with electron-withdrawing groups, which might be caused by the relatively higher electron densities of the alcoholic hydroxyl groups. Similarly, nitrobenzenes substituted with both electron-donating and

Table 2

Products and conversions of imines synthesis by CHT cascade reaction catalyzed by Co-ZnO/NC.

1f, 4 h, 94% ^[a] (97% ^[b]).	2f, 6 h, 90% (95%).	3f, 6 h, 94% (95%).
4f, 8 h, 78% (95%).	5f, 8 h, 81% (86%).	6f, 6 h, 96% (94%).
7f, 24 h, 68% (70%).	8f, 24 h, 88% (91%).	9f, 6 h, 81% (88%).
10f, 6 h, 88 % (95%).	11f, 6 h, 85%, (71%).	12f, 6 h, 50% (80%).

Reaction conditions: alcohols (denoted as a, 3 mmol), nitro compounds (denoted as b, 1 mmol), Co-ZnO/NC (20 mg), toluene (1 mL), 160 °C, N_2 . [a] Nitro-compounds conversions were determined by GC and [b] selectivities towards the aimed imines based on the yields and nitro-compounds conversions.

electron-withdrawing groups (entries 9f–12f) could be steadily transfer-hydrogenated into the corresponding imines by benzyl alcohol over Co-ZnO/NC, achieving moderate to high yields. Since the hydrogenation of nitrobenzene is not the rate-determining step, nitrobenzenes with both electron-withdrawing and electron-donating groups at the *para* position could be steadily hydrogenated to form the related imines at almost the same reaction rates. Conversely, nitrobenzenes with substituent groups at the *ortho* position exhibited lower conversions, likely due to steric effects.

4. Conclusion

A novel hierarchical nano-pyramid-like hybrid Co-ZnO/NC, where Co SAs were deposited on highly dispersed ZnO nanoparticles supported by an NC material, was prepared by calcining a bimetallic ZnCo-ZIF precursor with an appropriate Zn/Co ratio under an inert atmosphere. The hybrid showed an excellent catalytic performance toward the CHT cascade reaction between nitrobenzene and benzyl alcohol under an ambient inert atmosphere at 160 °C for 4 h with a nitrobenzene/benzyl alcohol molar ratio of 1/3. The nitrobenzene conversion and imine selectivity reached 94 % and 97 %, respectively, and the TOF (8.8 h^{-1}) was almost 15 times that reported for Co-N-C/CNT@AC. To the best of our knowledge, Co-ZnO/NC can be considered a state-of-the-art non-noble-metal catalyst for this reaction. The excellent catalytic activity of nano-pyramid Co-ZnO/NC is derived from the Co SAs supported on ZnO, which reduce the reaction barrier for hydroxyl dehydrogenation of the alcohol, facilitating the first and rate-determining step of the cascade reaction. Moreover, Co-ZnO/NC can be recycled several times without significant loss in CHT capacity after re-calcination under a N_2 atmosphere, and the catalyst exhibits good universality toward multiple benzyl alcohol and nitrobenzene derivatives, showing every aspect in industrial applications.

CCRediT authorship contribution statement

Chen Wu: Data curation, Writing - original draft. **Changyan Zhu:** Methodology, Software. **Kangkai Liu:** Formal analysis. **Shaowei Yang:** Software, Validation. **Yu Sun:** Investigation. **Kai Zhu:** Resources. **Yueling Cao:** Conceptualization, Project administration, Writing - review & editing. **Sai Zhang:** Writing - review & editing. **Sifei Zhuo:** Writing - review & editing. **Min Zhang:** Methodology, Supervision. **Qiuyu Zhang:** Funding acquisition. **Hepeng Zhang:** Conceptualization, Supervision, Project administration, Writing - review & editing.

Declaration of Competing Interest

The authors report no declarations of interest.

Acknowledgements

This work was financially supported by the Science and Technology Project of Shenzhen (No. JCYJ20190806155814624); the National Natural Science Foundation of China (No. 22002120) and the Guangdong Basic and Applied Basic Research Foundation (No. 2019A1515110507). We would like to thank the Analytical & Testing Center of Northwestern Polytechnical University for SEM, TEM, XRD, and XPS characterizations.

Appendix A. Supplementary data

Supplementary material related to this article can be found, in the online version, at doi:<https://doi.org/10.1016/j.apcatb.2021.120288>.

References

- [1] S. Kobayashi, H. Ishitani, Catalytic enantioselective addition to imines, *Chem. Rev.* 99 (1999) 1069–1094, <https://doi.org/10.1021/cr980414z>.
- [2] D. Chen, V. Leich, F. Pan, J. Klankermayer, Enantioselective hydrosilylation with chiral frustrated Lewis pairs, *Chem. Eur. J.* 18 (2012) 5184–5187, <https://doi.org/10.1002/chem.201200244>.
- [3] L. Yuan, L. Jiang, D. Thompson, C.A. Nijhuis, On the remarkable role of surface topography of the bottom electrodes in blocking leakage currents in molecular diodes, *J. Am. Chem. Soc.* 136 (2014) 6554–6557, <https://doi.org/10.1021/ja5007417>.
- [4] K.-i. Shimizu, K. Kon, M. Seto, K. Shimura, H. Yamazaki, J.N. Kondo, Heterogeneous cobalt catalysts for the acceptorless dehydrogenation of alcohols, *Green Chem.* 15 (2013) 418–424, <https://doi.org/10.1039/C2GC36555C>.
- [5] C. Bo, L. Wang, G. Shuang, Recent advances in aerobic oxidation of alcohols and amines to imines, *ACS Catal.* 5 (2015) 5851–5876, <https://doi.org/10.1021/acscatal.5b01479>.
- [6] Y. Wang, T. Wei, Y. Qu, Y. Zhou, Y. Zheng, C. Huang, Y. Zhang, Q. Yu, H. Chen, Smart, photothermally activated, antibacterial surfaces with thermally triggered bacteria-releasing properties, *ACS. Appl. Mater. Interface* 12 (2020) 21283–21291, <https://doi.org/10.1021/acsami.9b17581>.
- [7] Y. Bu, L. Zhang, J. Liu, L. Zhang, T. Li, H. Shen, X. Wang, F. Yang, P. Tang, D. Wu, Synthesis and properties of hemostatic and bacteria-responsive in situ hydrogels for emergency treatment in critical situations, *ACS. Appl. Mater. Interface* 8 (2016) 12674–12683, <https://doi.org/10.1021/acsami.6b03235>.
- [8] W. Xie, S. Huang, D. Tang, S. Liu, J. Zhao, Biomass-derived Schiff base compound enabled fire-safe epoxy thermoset with excellent mechanical properties and high glass transition temperature, *Chem. Eng. J.* 394 (2019) 123667, <https://doi.org/10.1016/j.cej.2019.123667>.
- [9] S. Xie, T. Xia, S. Li, C. Mo, M. Chen, X. Li, Bacteria-propelled microrockets to promote the tumor accumulation and intracellular drug uptake, *Chem. Eng. J.* 392 (2020) 123786, <https://doi.org/10.1016/j.cej.2019.123786>.
- [10] H. Schiff, Mittheilungen aus dem universitätslaboratorium in Pisa: Eine neue Reihe organischer Basen, *Justus Liebigs Ann. Chem.* 131 (1864) 118–119, <https://doi.org/10.1002/jlac.18641310113>.
- [11] G. Liu, D.A. Cogan, T.D. Owens, T.P. Tang, J.A. Ellman, Synthesis of enantiomerically pure N-tert-butanefulfinyl amines (tert-butanefulfinimines) by the direct condensation of tert-butanefulfinamide with aldehydes and ketones, *J. Org. Chem.* 64 (1999) 1278–1284, <https://doi.org/10.1021/jo982059i>.
- [12] H. Naeimi, F. Salimi, K. Rabiei, Mild and convenient one pot synthesis of Schiff bases in the presence of $\text{P}_2\text{O}_5/\text{Al}_2\text{O}_3$ as new catalyst under solvent-free conditions, *J. Mol. Catal. A: Chem.* 260 (2006) 100–104, <https://doi.org/10.1016/j.molcata.2006.06.055>.
- [13] M. Hosseini-Sarvari, Nano-tube TiO_2 as a new catalyst for eco-friendly synthesis of imines in sunlight, *Chin. Chem. Lett.* 22 (2011) 547–550, <https://doi.org/10.1016/j.cclet.2010.11.017>.
- [14] S. Biswas, B. Dutta, K. Mullick, C. Kuo, A.S. Poyraz, S.L. Suib, Aerobic oxidation of amines to imines by cesium-promoted mesoporous manganese oxide, *ACS Catal.* 5 (2015) 4394–4403, <https://doi.org/10.1021/acscatal.5b00325>.
- [15] V.S. Marakatti, S.C. Sarma, B. Joseph, D. Banerjee, S.C. Peter, Synthetically tuned atomic ordering in PdCu nanoparticles with enhanced catalytic activity toward solvent-free benzylamine oxidation, *ACS. Appl. Mater. Interface* 9 (2017) 3602–3615, <https://doi.org/10.1021/acsami.6b12253>.
- [16] X. Cui, W. Li, K. Junge, Z. Fei, M. Beller, P.J. Dyson, Selective acceptorless dehydrogenation of primary amines to imines by core-shell cobalt nanoparticles, *Angew. Chem. Int. Ed.* 59 (2020) 7501–7507, <https://doi.org/10.1002/anie.201915526>.
- [17] M. Rafiee, K.C. Miles, S.S. Stahl, Electrocatalytic alcohol oxidation with TEMPO and bicyclic nitroxyl derivatives: driving force trumps steric effects, *J. Am. Chem. Soc.* 137 (2015) 14751–14757, [https://doi.org/10.1016/0021-9517\(83\)90200-2](https://doi.org/10.1016/0021-9517(83)90200-2).
- [18] W. He, L. Wang, C. Sun, K. Wu, S. He, J. Chen, P. Wu, Z. Yu, Pt-Sn/ γ - Al_2O_3 -catalyzed highly efficient direct synthesis of secondary and tertiary amines and imines, *Chem. Eur. J.* 17 (2011) 13308–13317, <https://doi.org/10.1002/chem.201101725>.
- [19] C. Chen, R. Fan, M. Han, X. Zhu, Y. Zhang, H. Zhang, H. Zhao, G. Wang, Tunable synthesis of imines and secondary-amines from tandem hydrogenation-coupling of aromatic nitro and aldehyde over NiCo_5 bi-metallic catalyst, *Appl. Catal. B: Environ.* 280 (2021) 119448, <https://doi.org/10.1016/j.apcatb.2020.119448>.
- [20] B. Dutta, S. March, L.A. Achola, S. Sahoo, J. He, A.S. Amin, Y. Wu, S. Podes, S. P. Alpay, S.L. Suib, Mesoporous cobalt/manganese oxide: A highly selective bifunctional catalyst for amine-imine transformations, *Green Chem.* 20 (2018) 3180–3185, <https://doi.org/10.1039/C8GC00862K>.
- [21] J. Qin, Y. Long, W. Wu, W. Zhang, Z. Gao, J. Ma, Amorphous Fe_2O_3 improved [O] transfer cycle of $\text{Ce}^{4+}/\text{Ce}^{3+}$ in CeO_2 for atom economy synthesis of imines at low temperature, *J. Catal.* 371 (2019) 161–174, <https://doi.org/10.1016/j.jcat.2019.01.032>.
- [22] H. Zhang, C. Wu, W.L. Wang, J. Bu, F. Zhou, B. Zhang, Q. Zhang, Effect of ceria on redox-catalytic property in mild condition: a solvent-free route for imine synthesis at low temperature, *Appl. Catal. B: Environ.* 227 (2018) 209–217, <https://doi.org/10.1016/j.apcatb.2018.01.012>.
- [23] M. Tamura, K. Tomishige, Redox properties of CeO_2 at low temperature: the direct synthesis of imines from alcohol and amine, *Angew. Chem. Int. Ed.* 54 (2015) 864–867, <https://doi.org/10.1002/anie.201409601>.
- [24] J. Bu, W. Wang, H. Zhang, C. Wu, B. Zhang, Y. Cao, F. Zhou, Q. Zhang, X. Zhang, Efficient synthesis of imine from alcohols and amines over different crystal

- structure MnO_x catalysts, *Mol. Catal.* 459 (2018) 46–54, <https://doi.org/10.1016/j.mcat.2018.08.016>.
- [25] H. Shen, J. Bu, W. Wang, C. Wu, Y. Cao, B. Zhang, Q. Zhang, H. Zhang, Insight into Ce doping induced oxygen vacancies over Ce-doped MnO₂ catalysts for imine synthesis, *Chin. J. Chem.* 38 (2020) 1353–1359, <https://doi.org/10.1002/cjoc.202000155>.
- [26] S. Yang, H. Shen, F. Cheng, C. Wu, Y. Cao, S. Zhuo, Q. Zhang, H. Zhang, Organometallic precursor induced defect-enriched mesoporous CeO₂ with high specific surface area: Preparation and catalytic performance, *J. Mater. Chem. A* 8 (2020) 14006–14014, <https://doi.org/10.1039/D0TA02218G>.
- [27] X. Cao, J. Qin, G. Gou, J. Li, W. Wu, S. Luo, Y. Luo, Z. Dong, J. Ma, Y. Long, Continuous solvent-free synthesis of imines over uip- γ -Al₂O₃-CeO₂ catalyst in a fixed bed reactor, *Appl. Catal. B: Environ.* 272 (2020) 118958, <https://doi.org/10.1016/j.apcatb.2020.118958>.
- [28] J. Chen, S. Huang, J. Lin, W. Su, Recyclable palladium catalyst for facile synthesis of imines from benzyl alcohols and nitroarenes, *Appl. Catal. A: Gen.* 470 (2014) 1–7, <https://doi.org/10.1016/j.apcata.2013.10.033>.
- [29] L. Tang, H. Sun, Y. Li, Z. Zha, Z. Wang, Highly active and selective synthesis of imines from alcohols and amines or nitroarenes catalyzed by Pd/DNA in water with dehydrogenation, *Green Chem.* 14 (2012) 3423–3428, <https://doi.org/10.1039/C2GC36312G>.
- [30] D. Tan, H. Li, D.J. Young, J. Lang, Phosphine ligand-free RuCl₃-catalyzed reductive N-alkylation of aryl nitro compounds, *Tetrahedron* 72 (2016) 4169–4176, <https://doi.org/10.1016/j.tet.2016.05.036>.
- [31] S. Meenakshisundaram, Q. He, S.R. Dawson, E. Nowicka, L. Lu, P.C.A. Bruijninx, A.M. Beale, C.J. Kiely, B.M. Weckhuysen, Supported bimetallic nano-alloys as highly active catalysts for the one-pot tandem synthesis of imines and secondary amines from nitrobenzene and alcohols, *Catal. Sci. Technol.* 6 (2016) 5473–5482, <https://doi.org/10.1039/c6cy00425c>.
- [32] X. Cui, C. Zhang, F. Shi, Y. Deng, Au/Ag–Mo nano-rods catalyzed reductive coupling of nitrobenzenes and alcohols using glycerol as the hydrogen source, *Chem. Commun.* 48 (2012) 9391–9393, <https://doi.org/10.1039/c2cc34178f>.
- [33] C. Tang, L. He, Y. Liu, Y. Cao, H. He, K. Fan, Direct one-pot reductive N-alkylation of nitroarenes by using alcohols with supported gold catalysts, *Chem. Eur. J.* 17 (2011) 7172–7177, <https://doi.org/10.1002/chem.201100393>.
- [34] D. Liu, P. Yang, H. Zhang, M. Liu, W. Zhang, D. Xu, J. Gao, Direct reductive coupling of nitroarenes and alcohols catalysed by Co–N–C/CNT@AC, *Green Chem.* 21 (2019) 2129–2137, <https://doi.org/10.1039/C8GC03818J>.
- [35] W. Cheng, S. Akhter, H.H. Kung, Structure sensitivity in methanol decomposition on ZnO single-crystal surfaces, *J. Catal.* 82 (1983) 341–350, [https://doi.org/10.1016/0021-9517\(83\)90200-2](https://doi.org/10.1016/0021-9517(83)90200-2).
- [36] Y. Shinohara, T. Nakajima, S. Suzuki, A theoretical study of the dehydration and the dehydrogenation processes of alcohols on metal oxides using MOPAC, *J. Mol. Struct.: THEOCHEM.* 460 (1999) 231–244, [https://doi.org/10.1016/S0166-1280\(98\)00321-2](https://doi.org/10.1016/S0166-1280(98)00321-2).
- [37] M.V. Morales, E. Asedegbega-Nieto, A. Iglesias-Juez, I. Rodríguez-Ramos, A. Guerrero-Ruiz, Role of exposed surfaces on zinc oxide nanostructures in the catalytic ethanol transformation, *ChemSusChem* 8 (2015) 2223–2230, <https://doi.org/10.1002/cssc.201500425>.
- [38] Y. Zhang, Y. Yang, H. Han, M. Yang, L. Wang, Y. Zhang, Z. Jiang, C. Li, Ultra-deep desulfurization via reactive adsorption on Ni/ZnO: the effect of ZnO particle size on the adsorption performance, *Appl. Catal. B: Environ.* 119 (2012) 13–19, <https://doi.org/10.1016/j.apcatb.2012.02.004>.
- [39] X.K. Gu, C.Q. Huang, W.X. Li, First-principles study of single transition metal atoms on ZnO for the water gas shift reaction, *Catal. Sci. Technol.* 7 (2017) 4294–4301, <https://doi.org/10.1039/c7cy00704c>.
- [40] Y. Lee, S. Kim, S.Y. Jeong, S. Seo, C. Kim, H. Yoon, H.W. Jang, S. Lee, Surface-modified Co-doped ZnO photoanode for photoelectrochemical oxidation of glycerol, *Catal. Today* 359 (2021) 43–49, <https://doi.org/10.1016/j.cattod.2019.06.065>.
- [41] L. Yang, R. Ma, H. Zeng, Z. Rui, Y. Li, MOF-templated core-shell Co (II/III)@ ZnO hexagonal prisms for selective oxidation of vanillyl alcohol, *Catal. Today* 355 (2020) 280–285, <https://doi.org/10.1016/j.cattod.2019.02.031>.
- [42] Z. Lu, B. Wang, Y. Hu, W. Liu, Y. Zhao, R. Yang, Z. Li, J. Luo, B. Chi, Z. Jiang, M. Li, S. Mu, S. Liao, J. Zhang, X. Sun, An isolated zinc–cobalt atomic pair for highly active and durable oxygen reduction, *Angew. Chem. Int. Ed.* 58 (2019) 2622–2626, <https://doi.org/10.1002/anie.201810175>.
- [43] L. Rygh, O. Ellestad, P. Klæboe, C. Nielsen, Infrared study of CO adsorbed on Co/ γ -Al₂O₃ based Fischer–Tropsch catalysts; semi-empirical calculations as a tool for vibrational assignments, *Phys. Chem. Chem. Phys.* 2 (2000) 1835–1846, <https://doi.org/10.1039/B000188K>.
- [44] M. Jiang, N. Koizumi, T. Ozaki, M. Yamada, Adsorption properties of cobalt and cobalt-manganese catalysts studied by in situ diffuse reflectance FTIR using CO and CO + H₂ as probes, *Appl. Catal. A: Gen.* 209 (2001) 59–70, [https://doi.org/10.1016/S0926-860X\(00\)00755-9](https://doi.org/10.1016/S0926-860X(00)00755-9).
- [45] W.G. Cui, X.Y. Zhuang, Y.T. Li, H. Zhang, J.J. Dai, L. Zhou, Z. Hu, T.L. Hu, Engineering Co/MnO heterointerface inside porous graphitic carbon for boosting the low-temperature CO₂ methanation, *Appl. Catal. B: Environ.* 287 (2021) 119959, <https://doi.org/10.1016/j.apcatb.2021.119959>.
- [46] X. Xu, J. Luo, L. Li, D. Zhang, Y. Wang, G. Li, Unprecedented catalytic performance in amine syntheses via Pd/g-C₃N₄ catalyst-assisted transfer hydrogenation, *Green Chem.* 20 (2018) 2038–2046, <https://doi.org/10.1039/C8GC00144H>.
- [47] A. Mahata, R.K. Rai, I. Choudhuri, S.K. Singh, B. Pathak, Direct vs. indirect pathway for nitrobenzene reduction reaction on a Ni catalyst surface: a density functional study, *Phys. Chem. Chem. Phys.* 16 (2014) 26365–26374, <https://doi.org/10.1039/c4cp04355c>.
- [48] C. Morrissey, H. He, Silicene catalyzed reduction of nitrobenzene to aniline: a mechanistic study, *Chem. Phys. Lett.* 695 (2018) 228–234, <https://doi.org/10.1016/j.cplett.2018.02.027>.
- [49] S. Tian, M. Hu, Q. Xu, W. Gong, W. Chen, J. Yang, Y. Zhu, C. Chen, J. He, Q. Liu, H. Zhao, D. Wang, Y. Li, Single-atom Fe with Fe₁N₃ structure showing superior performances for both hydrogenation and transfer hydrogenation of nitrobenzene, *Sci. China Mater.* 64 (2021) 642–650, <https://doi.org/10.1007/s40843-020-1443-8>.
- [50] W. Xiong, Z. Wang, S. He, F. Hao, Y. Yang, Y. Lv, W. Zhang, P. Liu, Ha. Luo, Nitrogen-doped carbon nanotubes as a highly active metal-free catalyst for nitrobenzene hydrogenation, *Appl. Catal. B: Environ.* 260 (2020) 118105, <https://doi.org/10.1016/j.apcatb.2019.118105>.
- [51] M.D. Argyle, C.H. Bartholomew, Heterogeneous catalyst deactivation and regeneration: a review, *Catalysts* 5 (2015) 145–269, <https://doi.org/10.3390/catal5010145>.